J Therm Anal Calorim (2012) 109:39–47
DOI 10.1007/s10973-011-1324-0

Thermo-mechanical properties of snake-like NiTi wires and their use in miniature devices

Adelaide Nespoli · Elena Villa · Stefano Besseghini

Received: 22 November 2010 / Accepted: 6 January 2011 / Published online: 12 February 2011

Abstract In this study, we present the thermo-mechanical characterization of snake-like shape memory alloy (SMA) NiTi wires. Several samples were formed at different thermal treatments and analyzed through calorimetry and thermo-mechanical tests. It was found that for small deformations the snake-like SMA wire behaves as a quasi-elastic material, presenting the flag-shape pseudoelastic behavior at high thermal treatment temperatures. The mechanical performance seems to depend basically on the snake geometry instead on the thermal treatment; only for the 773 K treatment sample the performance rapidly gets worse. Stabilization is reached in few cycles. After the thermo-mechanical characterization, we studied the performance of the snake-like SMA wire mounted in a miniature rotational actuator, suggesting an innovative application in the actuator field.

Keywords Shape memory alloy · Snake-like shape · Miniature device · Rotational actuator

Introduction

The SMAs are intermetallic materials able to recover a deformation after a thermal cycle under a typical stress of 200–300 MPa [1, 2]. The mechanical work which results from this shape recovery is used in actuators to produce linear or rotational movement.

A. Nespoli (✉) · E. Villa · S. Besseghini
Consiglio Nazionale delle Ricerche – Istituto per l'Energetica e le Interfasi (CNR-IENI), U.O.S. di Lecco,
Corso Promessi Sposi 29, 23900 Lecco, Italy
e-mail: a.nespoli@ieni.cnr.it

Published scientific literature presents several studies in which SMAs are used as active element in linear or rotational mini-actuators, in the straight or the helical spring shapes [3–13]. In a recent review paper [14], we argued that at present there is a sort of limitation in fabricating SMA miniature actuator and we concluded that there is a great potential for further optimization. Innovative SMA wire shapes could shift the current virtual technological limit nearer to the ideal functioning condition.

In this study, an alternative way of forming the SMA element, the snake-like shape, is presented. This conformation is quite uncommon in the actuator field; very few applications can be found in textile and medical domains [15–17]. Several different kinds of snake-like SMA wires are presented; each sample is took under a set of thermal treatments and then analyzed by calorimetric and mechanical tests [18–20]. A new application of the snake-like SMA wire in the miniature rotational actuator field is finally presented.

Experimental

Snake-like SMA wire samples were obtained from a polycrystalline commercial NiTi wire (Global System s.r.l.), having the diameter of 200 μm. A snake-like wire is characterized by four parameters: the high, H, the curvature radius, R, the distance between two consecutive curvatures, D, and the number of curvatures, N (see Fig. 1). In this study, samples having the straight ends belonging to two parallel and not coincident axes were studied (in this case N assumes only even values).

Two main different kinds of geometries were considered, the small, S, and the large, L, one; H, R, and D mean

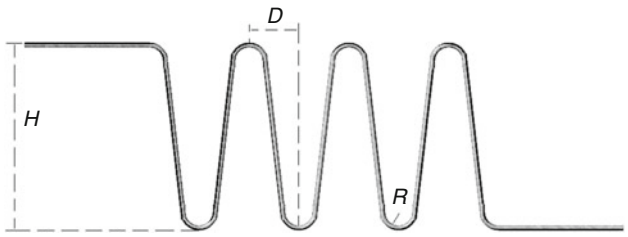

Fig. 1 Example of a snake-like wire with six curvatures ($N = 6$): H is the high, R is the radius of curvature, and D is the distance between two consecutive curvatures

Table 1 High H, radius of curvature R, and distance between two consecutive curvatures D mean values of the large, L, and small, S, snake-like geometry

Geometry	H/mm	R/mm	D/mm
L	6.91 ± 0.07	0.72 ± 0.02	2.01 ± 0.09
S	5.27 ± 0.07	0.54 ± 0.03	0.82 ± 0.06

values corresponding to these two shapes are reported in Table 1.

For each geometry, two subsets of samples were analyzed: the first one comprises samples with two curvatures ($N = 2$) and the second includes specimens having four curvatures ($N = 4$).

Figure 2 shows two examples of snake-like SMA wires: the one on the left has the L geometry and two curvatures ($N = 2$) while the one on the right has the S geometry and four curvatures ($N = 4$).

In order to give the specimens the snake shape, the NiTi wire was mounted on a specific tools made of an aluminum drilled bar; a certain amount of nails were used to fix the SMA wire in the snake-like arrangement. Each sample was then thermal treated at different temperatures, 573, 623, 673, 723, 773, and 1023 K for 10 min and then water quenched (wq) at room temperature.

After the thermal treatment, each sample was analyzed by differential scanning calorimetry (DSC) using a DSC/220 Seiko Instruments device equipped with a liquid nitrogen cooling system, to assess the martensite and austenite transformation temperatures and the transformation latent heat during cooling and heating as a function of the thermal treatment temperature. Each DSC measurement was conducted in the 193–393 K range with a rate of 10 K/min. DSC samples were prepared to have a mass between the limits required for the used DSC instrument (3–50 mg); in Table 2, the mass of the samples used in the calorimetric measurements is reported.

A series of tensile tests were used to study the mechanical behavior of the samples using the Dynamic Mechanical Analyzer DMA Q800 TA Instruments equipped with a liquid nitrogen cooling system. In the first set of experiments, the force *versus* strain curves of the austenite and the martensite phase as a function of the thermal treatment were studied separately, by measuring the loading and unloading force in the 0–10 mm deformation range at a constant temperature of 193 K for the martensite and 358 K for the austenite. Each sample underwent to three mechanical cycles. The skill of this test was to assess the mechanical response only of the sample curvatures by solicited the specimens in a restricted range of deformation. After that, the mechanical response of the material was analyzed by deforming each sample up to 17 N of force which is the maximum force expressed by the test instrument. With this second tensile test, the mechanical contribution derived from the stress-induced martensite (SIM) was investigated. After this second test, the maximum stroke as function of the applied load was analyzed by varying the test temperature in the range between 193 and 423 K, under three different loads: 0.1, 0.2, and 0.3 N. Two thermal cycles were performed under these loads. Finally, the mechanical fatigue under a constant load (0.1 N) is studied.

After the thermo-mechanical characterization, two snake-like SMA wires with the S geometry and $N = 3$ were mounted in a miniature device composed by a box, two bearings, a shaft and some means to fix the snake-like SMA wires. This device has an overall volume of 1 cm^3 ($8 \times 25 \times 5$ mm^3) and a weight of 1.13 g. A thermo-mechanical characterization of the actuator is presented.

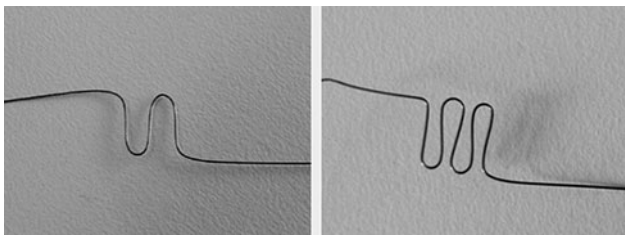

Fig. 2 Example of snake-like SMA wires. On the left, L snake-like SMA wire with $N = 2$; on the right, S snake-like SMA wire with $N = 4$

Table 2 Mass of the samples analyzed through differential scanning calorimetry for different thermal treatment temperatures

Thermal treatment temperature/K × 10 min, wq	Mass/mg
573	8.96
623	9.57
673	7.53
723	6.86
773	6.53
1023	9.75

Results

Figure 3 shows the DSC curves of the samples thermal treated at the temperatures reported in the Experimental section. It can be seen that DSC curves change strongly depending on the thermal treatment temperature. During cooling, two almost indiscernible peaks are visible at low temperatures. These peaks are associated to two distinct martensitic transformations: the first is related to B2-R and the second to R-B19′ transitions (B2, R, and B19′ stand for the cubic, the rombohedral, and the monoclinic structures, respectively). The areas under these peaks represent the correspondent phase transformation latent heat [2]. These peaks become sharper with the increasing of the treatment temperature and the range of temperature in which two phases coexist becomes smaller for high temperatures. An analogous behavior is visible during heating.

Figure 4 shows the trend of the phase transformation temperatures as a function of the thermal treatment temperatures; all transition temperatures were derived from the DSC curves using the tangent method [21]. In this figure *R*, *M*, and *A* stand for rombohedral, monoclinic, and austenite structure temperature, respectively while *s* and *f* stand for transformation starting and finishing point. In this figure is also reported the transformation latent heat normalized to the sample mass. It can be seen that during cooling (a) the rombohedral starting and finishing temperatures are independent of the treatment temperature while the monoclinic starting and finishing temperatures shift to higher values when the thermal treatment temperature gets near to the fully annealed one (i.e., 1023 K) where no rombohedral structure is still visible. Analogous comments can be done for the reverse transformation. The transformation latent heat increases (decreases) heating (cooling) till the 773 K treatment after which it shows an almost constant trend. The transformation latent heat limits reported in Fig. 4 are typical of the NiTi system [22]. The trend depicted in Fig. 4c is due to dislocations derived from the cold working process; dislocations generate internal stresses which inhibit martensite from transforming into austenite, so the latent heat is low for low treatment temperatures. Dislocations annihilate during thermal treatments; increasing the treatment temperature dislocations are removed and latent heat increases [23].

Figure 5 shows the first set of mechanical test conducted in the 0–10 mm deformation range. The figure shows the static force *versus* strain curves of austenite (black lines) and of martensite (gray lines) phase of samples having the *S* and *L* geometries, $N = 4$ and subjected to the thermal treatments we previously listed, excluded the fully annealed one. It can be seen that the unloading force of the first mechanical cycle of each sample does not close to zero. This behavior is caused by the internal stresses which disappear after the first thermo-mechanical cycle. After the first cycle, each sample shows a quasi-complete recovery of the deformation both in the austenite and in the martensite phase. In the range of deformation considered in this test, 0-–0 mm, the registered austenite and martensite maximum force appears to depend strongly on the sample geometry

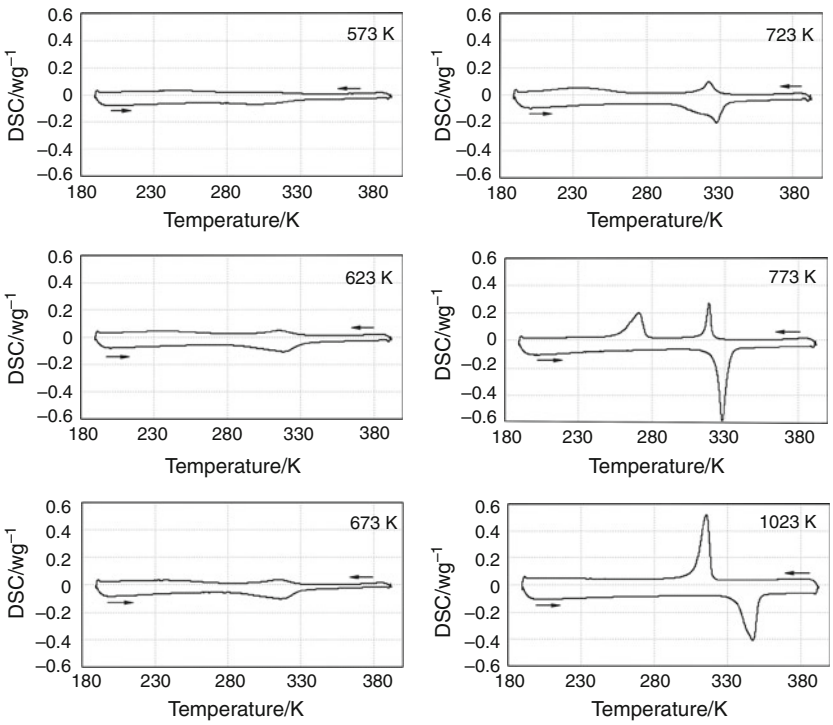

Fig. 3 DSC curves for different thermal treatment temperature, 573, 623, 673, 723, 773, and 1023 K for 10 min (samples were water quenched after each heat treatment); heating/cooling rate was set to 10 K/min

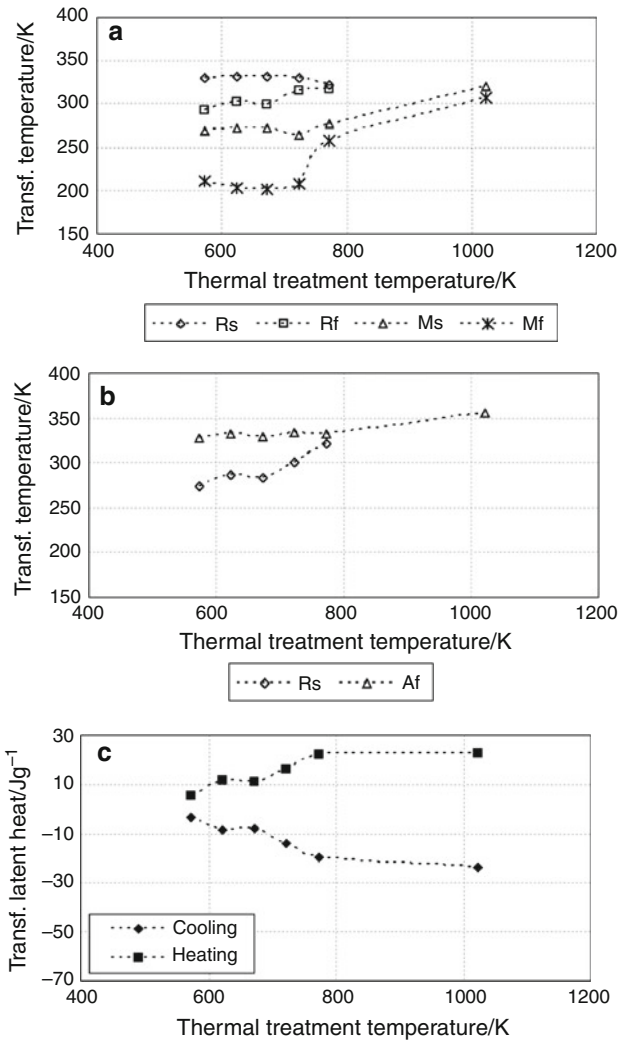

Fig. 4 DSC analysis results. Phase transformation temperatures during cooling (**a**) and heating (**b**) and transformation latent heat normalized to the mass (**c**) as a function of the thermal treatment temperatures

instead on the thermal treatment temperature. For high temperatures, it can be seen that the *S* snake-like wire shows the characteristic flag-shaped pseudoelastic behavior.

Figure 6 depicts the static force as a function of the displacement of the specimens having the *L* geometry and $N = 2$, up to 17 N of force. In this figure, we can see that the force shows two main mechanical responses: the first one is the elastic response of the snake wire during the opening of the curvatures visible for small deformations, the second one is the mechanical behavior of the snake when all the curvatures are completely opened (i.e., the sample shape is similar to a straight wire). The deformation value at which the snake wire starts the second mechanical response increases with the increasing of the thermal treatment temperatures as the curvatures stiffness diminishes at high annealing temperatures.

Figure 7 shows the maximum stroke reached by the snake wire as a function of the applied load registered in the first mechanical cycle. Samples having the *L* geometry and $N = 4$ are not reported because for these samples the deformation exceeded the maximum limit displacement proposed by the testing machine. In this figure, it can be noted that the three samples show a similar trend. In particular, the *S* and the *L* geometry samples with $N = 2$ have the same mechanical behavior except for the *S* geometry sample treated at 623 K which performs better than the *L* one. We can also notice that the thermal treatment conducted at 773 K brings to a loss of performance for all the specimens. In general, the sample having the *S* geometry and $N = 4$ is the one showing the best mechanical performance.

In Fig. 8 is reported the mechanical fatigue (10000 load cycles) under the constant load of 0.1 N for the sample having the *S* geometry, $N = 4$ and thermal treated at 773 K. This sample stabilizes at 8 mm of stroke in few cycles. It can be also noticed that there is a shift of the recoverable deformation which stabilizes after about 4000 mechanical cycles.

Mechanical performance of the snake-like SMA wire mounted in a miniature rotational actuator

Two snake-like NiTi wires having the *S* geometry, $N = 4$ and thermal treated at 773 K were mounted one above the other in the foolproof device depicted in Fig. 9, acting as antagonists to produce a rotational movement in the two main directions. The overall device volume is 1 cm^3 ($8 \times 25 \times 5$ mm^3) and the weight is 1.13 g. The two straights parts of each snake sample were crimped to the shaft and to the box and the activation is obtained by joule effect by a supply current of 0.6 A for 5 s and a maximum power consumption of about 1 W. The electrical connections are represented by three external pins which are connected to the two straight ends of each snake wire and to the shaft which in turn acts as an electrical common pole. During the rotational movement, the straight snake end fixed to the shaft partially wounds around it.

Before starting the mechanical characterization of the device, we first evaluated the friction during the rotational movement, by comparing the snake wire displacement evaluated in two different conditions: during its regular functioning inside the device and during a standard tensile test conducted in similar loading and geometrical conditions; 3500 cycles were considered. In Fig. 10 is reported on the left the rotational angle of ROTOsma-1 under the constant torque of 0.1 Nmm and on the right the correspondent rotational angle mathematically derived from the maximum stroke evaluated with a tensile test under a constant load of 0.26 N (which is the maximum load

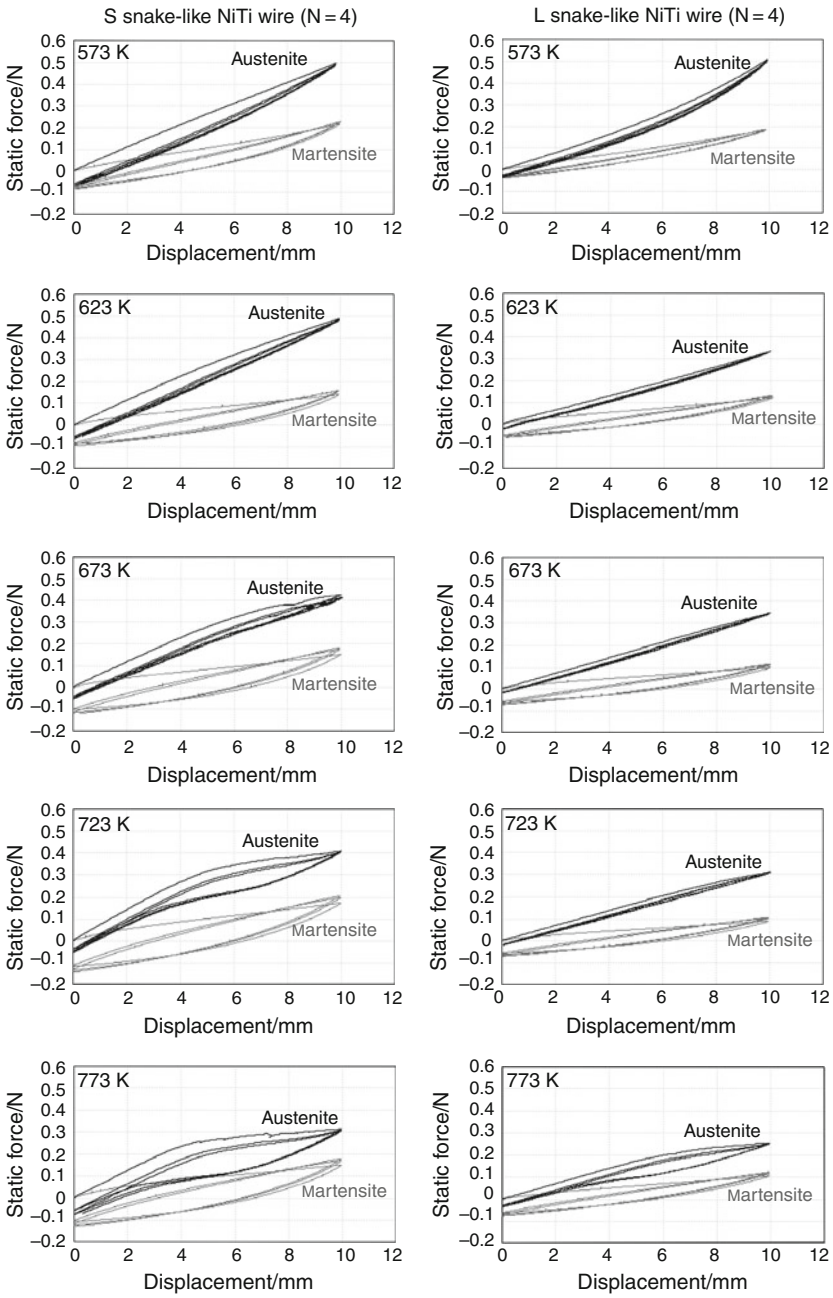

Fig. 5 Force *versus* displacement of the austenite (*black line*) and of the martensite (*gray line*) phase of the *S* (on the left) and *L* (on the right) geometries having $N = 4$, thermal treated at 573, 623, 673, 723, and 773 K for 10 min and water quenched at room temperature

transmitted to the snake wire when 0.1 Nmm is applied on the device shaft). For this last test mechanical stops were used to simulate the functioning in the actuator. Figure 10 shows that friction does not evidently alter the overall mechanical performance of the device as the rotational angles registered during the two tests are very similar. This means that the snake-like SMA wire performs in the actuator in the best way. It can be seen that the snake elements stabilize at a rotational angle of about 120° and that the shift of the recoverable strain stops at after about 500 cycles.

Discussion

The skill in recovery a pre-determinated shape is the main advantage in the use of SMA materials in the actuator field [24]. The actuator can express an amount of maximum force and stroke which strictly depends on the active element and on the mechanical parts. Hypothesizing that no friction occurs during the activation, it makes sense to attribute to the active element (i.e., the SMA element) the whole responsibility of the good mechanical functioning [25].

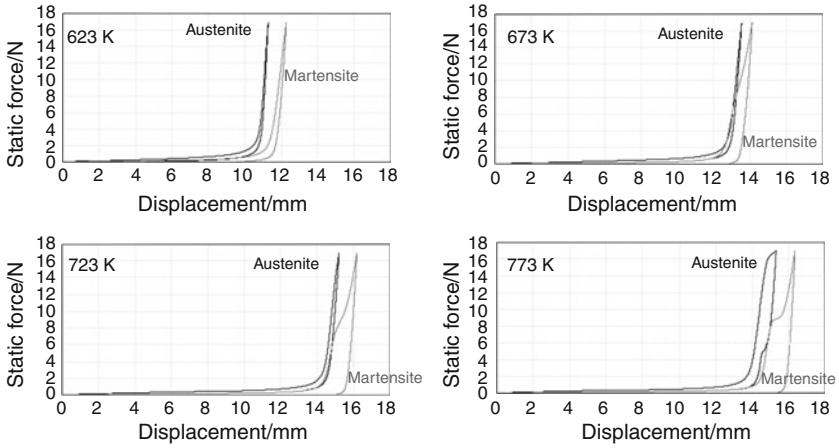

Fig. 6 Force *versus* displacement of the austenite (*black line*) and of the martensite (*gray line*) phase of *L* geometry samples with $N = 2$, thermal treated at 623, 673, 723, and 773 K for 10 min and water quenched at room temperature

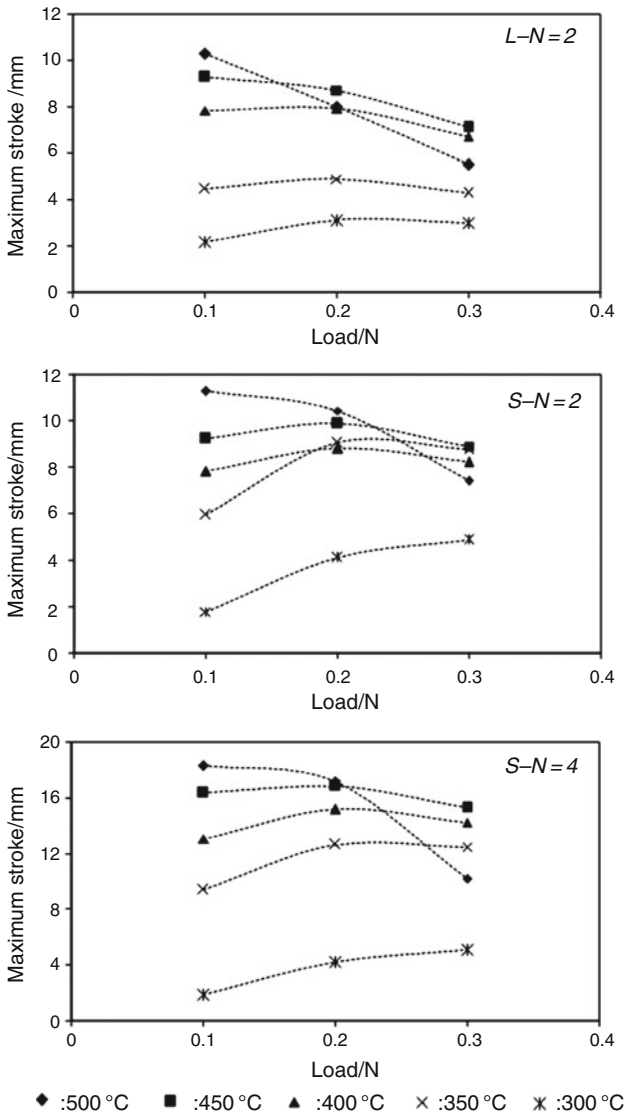

Fig. 7 Maximum stroke *versus* applied load of all the snake-like SMA wire samples we considered in this study, except the one having the *L* geometry and $N = 4$

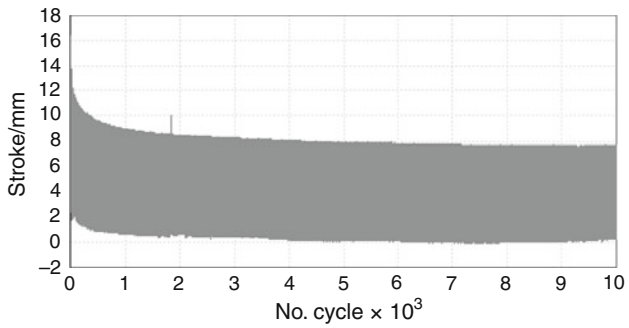

Fig. 8 Mechanical fatigue (10000 load cycles) under a load of 0.1 N for the *S* geometry sample having $N = 4$ and thermal treated at 773 K; room temperature was set to 298 K

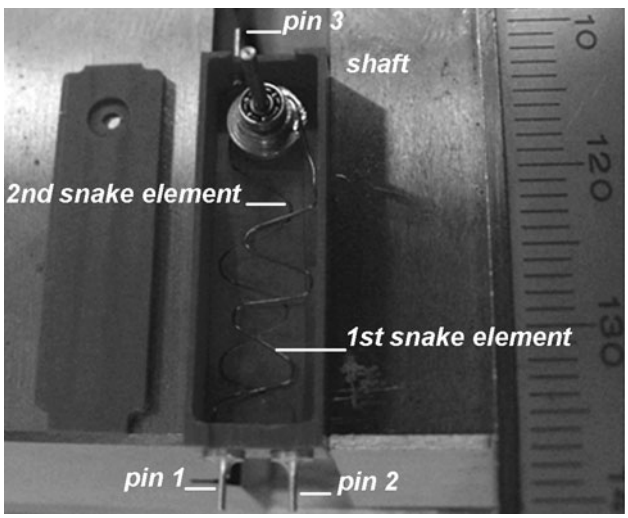

Fig. 9 Rotational mini-actuator used to test the snake-like SMA wires

When the geometrical volume dedicated to contain the active parts is fairly small, it's important to know the amount of the predefined actuator characteristic output

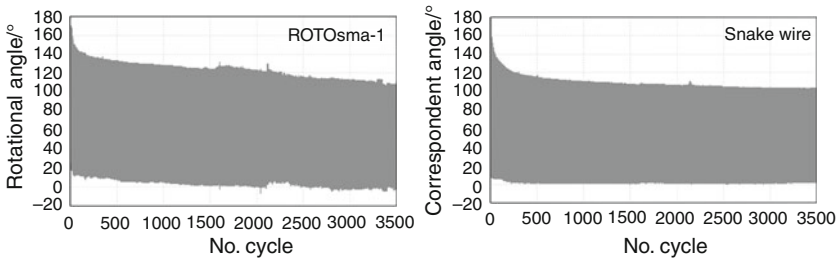

Fig. 10 Evaluation of the SMA device friction during cycling. Comparison between the rotational angle under a torque of 0.1 Nmm of ROTOsma-1 (*on the left*) and the correspondent angle derived from a standard tensile test (*on the right*); room temperature was set to 298 K

force and stroke suitable for the final use. Once we know these two functional requirements, we have to decide which SMA element shape fits the desired application. In this study, we suggest a new kind of SMA wire configuration, consisting in a planar wavy formed NiTi wire, we called snake-like SMA wire. This unusual shape is in general used in the biomedical and the textile field, where SMA or pseudoelastic thin wires are considered, but is fairly uncommon in the actuator branch. Due to its particular space arrangement, this new SMA wire conformation gives a chance to develop an actuator of quite small geometrical volume.

In this study, the snake elements are made of a commercial NiTi wire. A calorimetric study was done to know the theoretical maximum temperature (Af) reached by the snake wire (Figs. 3 and 4) which is very important when the snake element is used in a device; an increasing of temperatures due to the applied stress was neglected as the considered stresses are very low. From these two figures, it can be seen that the treatment which lead to good thermal properties is the 773 K one; in fact the 773 K treated sample is easily deformed at room temperature as it is quasi transformed into martensite and when it is heated it reaches a reasonable temperature (about 333 K).

Mechanical tests show that when deformed in the elastic region (Fig. 5), samples having the *S* and *L* geometry and $N = 4$ express a similar maximum force for each thermal treatment considered. After the first cycle, all specimens also show a complete recovery of the deformation both for austenite and for martensite, meaning that the elastic component is fairly strong for both them. Starting from the samples treated at 673 K, we can observe for the *S* geometry the flag-shaped pseudoelastic hysteresis. This means that only for these treatments the microstructure is suitable to induce martensite from parent phase by stress applied.

The elastic region of the snake-like SMA wire varied with the temperature of the thermal treatment, being small and large for low and high treatment temperature, respectively. We can see these discrepancies in Fig. 6 where the deformation at which the force begins a rapid increase shifts to high values as the samples treated at low temperature are less deformable than the one treated at high temperatures. This means that the curvature stiffness takes strongly part in the viscoelastic behavior of the snake-like SMA wire. For the austenite phase, the flag-shaped pseudoelastic hysteresis is visible only for the specimen treated at 773 K, while the detwinned martesite is quite evident from the treatment conducted at 673 K. From this test, we can also point out that the regions of maximum curvature of the wires are not mechanical fragile as no mechanical fracture occurs during these tests.

From Fig. 7, we can see that the thermal treatments conducted at 673 and 723 K grant the best mechanical performance, while the treatment conducted at 773 K leads to a drop off of the mechanical performance for loads higher than 0.1 and 0.2 N for *L* and *S* geometry, respectively. The mechanical stability is reached in few cycles, as reported in Fig. 8.

When embedded in a simple miniature mechanical device, the snake-like SMA wire does not lose its good mechanical performance and give a chance to the developing of new smart actuators. In particular, we presented a rotational miniature actuator in which the deformation of the snake element never exceeds 6 mm thanks to the geometry of the apparatus. Two identical *S* snake NiTi wires treated at 773 K were mounted to produce the rotational movement in the two main directions. Even though this thermal treated induces a loss of mechanical performance, see Fig. 7, it represents the best choice for ROTOsma-1: first of all because the NiTi wire must not be too stiff as the straight snake end fixed to the shaft partially wounds around it. Then because the two snake elements act as mutual antagonist; it was found that sample with a thermal treatment temperature lower than 773 K cannot deform the correspondent antagonist snake wire.

Comparing Figs. 8 and 10, we can see that the shift of the recoverable deformation is evidently reduced when the snake element is used in the device even though the load transmitted to the snake element is higher in the latter case. This is due to the deformation of the snake element which

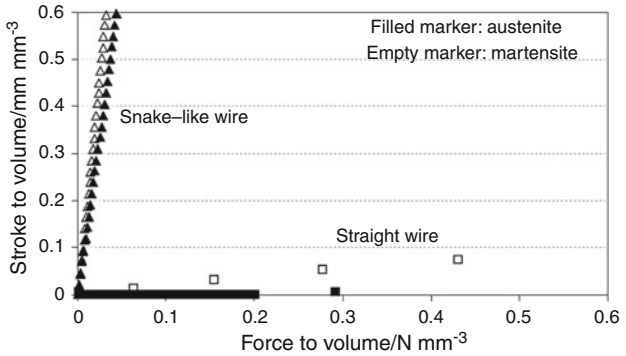

Fig. 11 Stroke-to-volume *versus* force-to-volume of snake-like wire and straight wire

never exceeds 6 mm inside ROTOsma-1; with a controlled deformation, the growth of plastic deformation is prevented and the recoverable strain stabilizes in a reduced number of cycles.

The friction between the snake SMA element and the shaft is limited by avoiding the phase transformation of the SMA wire segment which wounds around the shaft during the rotational movement, because this segment is always at zero potential.

The good performance of the actuator is strictly connected to the snake-like wire element. Due to the small geometrical volume, during the rotational movement the applied torque effect is transmitted only to the curved part of the snake wire producing a bend/unbend movement of the curvatures. Consequently, the straight segments which connect two consecutive curvatures, indirectly participate to the overall stroke of the snake wire as the transmitted stress does not cause the correspondent martensite deformation. The length of these straight segments is related to the high H of the snake wire; lower is H lower is the stroke of the snake wire but higher is the generated force as the snake shape becomes more similar to a straight wire. The stroke gain and the force loss deriving from the use of the snake shape can be seen in Fig. 11 which shows the mechanical performance derived from a standard tensile test of the snake like wire used in the actuator with a straight wire which was chosen in order to have the same elemental composition, the same thermal history, and the same diameter of the snake element of the snake wire and with a length compatible with the available space inside our actuator (i.e., 18 mm).

Conclusions

The snake-like shape represents a new way of forming SMA wire. We presented an experimental investigation of the mechanical performance of this unusual SMA geometry. The results show that the snake wire can generate an elastic behavior in a very large range of deformation comparing to the straight SMA wire. This point is very beneficial for practical use since the new proposed SMA wire just occupies small space to generate the same displacement as a straight SMA wire.

References

1. Funakubo H. Shape memory alloys. London: Gordon and Breach Science Publishers; 1984.
2. Otsuka K, Wayman CM. Shape memory materials. Cambridge: Cambridge University Press; 1998.
3. Jansen S, Breidert J, Welp EG. Positioning actuator based on shape memory wires. Proceedings Actuator 2004.
4. Strittmatter J, Gümpel P. Shape memory actuator for hydraulic valve. Proceedings Actuator 2004.
5. Pulnev S, Vahhi I, Priadko A, Rogov A. Miniature linear actuators based on Cu–Al–Ni shape memory single crystals. Proceedings on SMST 2004.
6. Priadko A, Pulnev S, Viahhi I. Actuator based on Cu–Al–Ni single crystals. Proceedings on SMST 2000.
7. Haga Y, Makishi W, Iwami K, Totsu K, Nakamura K, Esashi M. Dynamic braille display using SMA coil actuator and magnetic latch. Sens Actuators A. 2005;119:316–22.
8. Velázquez R, Pissaloux E, Szewczyk J. Miniature shape memory alloy actuator for tactile binary information display. Proceedings on IEEE-ICRA 2005.
9. Colli M, Bellini A, Concari C, Toscani A, Franceschini G. Current-controlled shape memory alloy actuators for automotive tumble flap. Proceedings IECON 2006.
10. Elwaleed AK, Mohamed NA, Mohd Nor MJ, Mohd MM. A new concept of a linear smart actuator. Sens Actuators A. 2007; 123:244–9.
11. Park BH, Shantz M, Prinz F. Scalable rotary actuators with embedded shape memory alloy. Proceedings on SPIE, vol 4327. 2001. pp. 78–87.
12. Pöhlau F, Meier H. Extremely compact high-torque drive with shape memory actuators and strain wave gear Wave Drive®. Proceedings on Actuator 2004.
13. Sharma SV, Nayak MM, Dinesh NS. Modelling, design and characterization of shape memory alloy-based poly-phase motor. Sens Actuators A. 2008;147:583–92.
14. Nespoli A, Besseghini S, Pittaccio S, Villa E, Viscuso S. The high potential of shape memory alloy in developing miniature mechanical devices: a review on shape memory alloy mini-actuators. Sens Actuators A. 2010;158:149–60.
15. Villa E, Arnaboldi S, Tuissi A, Giacomelli M, Turco E. Mechanical analysis of hybrid textile composites with NiTi wires. J Mater Eng Perform. 2009;18(5–6):517–21.
16. Mineta T, Mitsui T, Watanabe Y, Kobayashi S, Haga Y, Esashi M. Batch fabricated flat meandering shape memory alloy actuator for active catheter. Sens Actuators A. 2001;88:112–20.
17. Mineta T, Mitsui T, Watanabe Y, Kobayashi S, Haga Y, Esashi M. An active guide with shape memory alloy bending actuator fabricated by room temperature process. Sens Actuators A. 2002;97–98:632–7.
18. Nespoli A, Besseghini S. A complete thermo-mechanical study of a NiTiCu shape memory alloy wire. J Therm Anal Calorim. 2010. doi: 10.1007/s10973-010-1042-z.

19. Degeratu S, Rotaru P, Manolea Gh, Manolea HO, Rotaru A. Thermal characteristics of Ni–Ti SMA (shape memory alloy) actuators. J Therm Anal Calorim. 2009;97:695–700.
20. Artiaga R, Garcıa A, Garcıa L, Varela A, Mier JL, Naya S, Grana M. DMTA study of a nickel-titanium wire. J Therm Anal Calorim. 2002;70:199–207.
21. Shaw JA, Kyriakides S. Thermomechanical aspects of NiTi. J Mech Phys Solids. 1995;43:1243–81.
22. Wang G, Jiang XX, Nikanpour D. Measurement of specific heat, latent heat and phase transformation temperatures of shape memory alloys. High Temp High Press. 2008;37:91–107.
23. Wang ZG, Zu XT, Feng XD, Zhu S, Zhou JM, Wang LM. Annealing-induced evolution of transformation characteristics in TiNi shape memory alloys. Physica B. 2004;353:9–14.
24. Reynaerts D, Van Brussel H. Design aspects of shape memory actuators. Mechatronics. 1998;8:635–56.
25. Huang W. On the selection of shape memory alloys for actuators. Mater Des. 2002;23:11–9.